SIMULATION ANALYSIS OF AN AUTOMOTIVE ELECTROMAGNETIC SUSPENSION SYSTEM FOR ENHANCED VEHICLE STABILITY

M. Hui[1,2] and H. M. Ali[3,4*]

[1] School of Automotive Engineering, Dongying Vocational College of Science and Technology, Guangrao County, Dongying, Shandong, 257335, CHINA

[2] Faculty of Engineering, City University Malaysia, Cyberjaya Campus, 3500, Jalan Teknokrat 3, Cyber 4, Cyberjaya, Selangor Darul Ehsan, 63000, MALAYSIA

[3] Department of Aerospace Engineering, Faculty of Engineering, Universiti Putra Malaysia, UPM Serdang, Selangor Darul Ehsan, 43400, MALAYSIA

[4] Aerospace Malaysia Research Centre (AMRC), Level 7, Tower Block, Faculty of Engineering, Universiti Putra Malaysia, UPM Serdang, Selangor Darul Ehsan, 43400, MALAYSIA

Corresponding Author's Email: hidayatullah@upm.edu.my

Article History: Received 12 November 2025; Revised 13 December 2025; Accepted 29 December 2025

ABSTRACT: This study presents a simulation-based analysis of an electromagnetic active suspension system integrated with a proportional-integral-derivative (PID) control strategy, aimed at improving vehicle stability and ride comfort. The system, which is based on the traditional McPherson passive suspension structure, is designed to control suspension performance quickly without contact and friction. The effectiveness of the system is evaluated through MATLAB/Simulink simulations using a half-vehicle, four-degree-of-freedom model to assess dynamic behavior under varied driving conditions. Key performance indicators such as body acceleration, pitch angle acceleration, and suspension travel were examined to quantify improvements. The proposed system achieved reductions of 27% in body acceleration, 22% in pitch angle acceleration, 17% in front suspension travel, and 42.4% in rear suspension travel compared to conventional suspension setups. This research showing improvements in handling, ride comfort, and system adaptability to road conditions. In addition to improved vehicle dynamics, the design contributes to lower maintenance needs and reduced environmental impact, making it a promising framework for the development of advance automotive suspension technologies aimed at improving safety, comfort, and energy efficiency.

KEYWORDS: *Electromagnetic Suspension; PID Control; Ride Comfort;Vehicle Stability;Suspension Travel*

1.0 INTRODUCTION

The continuous pursuit of vehicle stability and ride comfort has intensified interest in advanced suspension technologies capable of overcoming the inherent limitations of conventional mechanical systems [1-2]. Electromagnetic suspension springs have gained significant attention due to their ability to provide precise and real-time adjustments of suspension characteristics through controlled electromagnetic forces [3-4]. This technology promises superior handling, improved ride quality, and adaptability across

varying road conditions, making it a strong candidate for modern intelligent automotive applications. However, challenges such as design complexity, high production costs, and material limitations continue to hinder widespread implementation. These unresolved technical and practical constraints leave the potential of electromagnetic suspension systems at a critical stage of research and development.

Recent advancements in electromagnetic suspension technology have significantly expanded the potential of active and semi-active vehicle suspension systems. Gysen et al. [5] introduced an electromagnetic active suspension system that integrates a permanent magnet linear actuator control performance with a continuous force output of 755 N at 1 m/s and a maximum force of 4 kN at 0.1 m/s. Building upon this foundation, Asadi et al. [6] developed a novel electromagnetic hybrid damper combining a viscous medium with an electromagnetic generator, achieving a high damping coefficient suitable for full-vehicle applications. Xiao et al. [7] further emphasized the benefits of pavement energy recovery systems, which contribute to improved vehicle fuel efficiency through the capture of road-induced vibrational energy.

In another innovative approach, Xing et al. [8] employed a linear motor actuator capable of precise electromagnetic force control, effectively facilitating efficient electric energy conversion. Zuo et al. [9] and Scully et al. [10], both proposed a four-phase machine design characterized by compact structure and high reliability, although it was noted to suffer from low energy conversion efficiency and inertial losses. More recently, Ding et al. [11] introduced a cylindrical transverse flux linear motor that aligned well with simulation predictions from Maxwell software, validating its design accuracy. Prajwal et al. [12] presented a two-way electromagnetic actuator that demonstrated small size, low weight, ease of control, and the capacity to improve vehicle handling across various road conditions. Their work also highlighted the benefits of dynamic adjustment of elastic stiffness to reduce vehicle tilt and vibration during high-speed maneuvers, thereby enhancing safety and comfort.

Research into energy harvesting suspensions has also progressed, as seen in the work of Pu et al. [13], who designed a ball screw shock absorber, though they reported that device inertia negatively affected damping performance and energy feed efficiency. Xie et al. [14] examined a damper integrating a ball screw and generator gearbox, capable of adjusting damping characteristics but limited under low-frequency excitation. Zhang et al. [15] introduced an electro-hydraulic damper, maintaining energy conversion efficiency at approximately 60%. Chen et al. [16] applied linear quadratic gaussian (LQG) control to modulate the damping force by adjusting circuit cell numbers, while Gao et al. [17] designed a PI-regulated energy feed circuit that achieved effective damping coefficient regulation and energy management.

In addition, Darabseh et al. [18] investigated piezoelectric stacks installed in series with suspension springs, achieving notable increases in harvest voltage and power output in semi-car models. Most recently, Yan and Yan [19] optimized proportional-integral-derivative (PID) controller parameters using a swarm optimization algorithm, which significantly improved vehicle acceleration responses, reduced suspension dynamic travel, and lowered peak tire dynamic load under varied road conditions. Similarly,

Solihin et al. [20] demonstrated that PID controllers optimized using Particle Swarm Optimization (PSO) achieved lower overshoot compared to those designed with the classical Zeigler-Nichols (Z-N) method. Among the PSO-based controllers, similar performance was observed except for the integral-time-square-error (ITSE) optimized controller, which showed a longer settling time. The study highlighted that while the classical method is useful for initial parameter estimation, modern optimization techniques like the PSO significantly improve controller performance.

Despite the progress of electromagnetic suspension spring technology, there remain significant challenges in its practical application. The design of electromagnetic suspension springs involves complexity in material selection, structural optimization, and electromagnetic field control, which directly affect the system's stiffness and damping characteristics. Additionally, problems such as the high cost of production, process limitations, environmental adaptability, and reliability under vibration and impact have not been fully resolved. These issues create a gap between theoretical development and practical vehicle-level application, especially in ensuring long-term durability and consistent performance on varying road surfaces. Furthermore, the industry still requires more detailed studies focusing on optimizing systems, such as PID controllers, to meet the demands of intelligent and energy-efficient automotive platforms.

To address these limitations, this study aims to design and simulate an electromagnetic suspension spring system integrated with a PID control strategy based on the half-car model. Ussing MATLAB for numerical modeling and dynamic simulation, the research investigates the influence of control parameters on the mechanical properties of the suspension system, such as body acceleration, pitch angle acceleration, and front and rear suspension travel. The objective is to enhance vehicle handling performance, body stability, and emergency response capability under various road condition. This approach intends to provide valuable insights for improving ride comfort and safety in modern vehicles, particularly for applications in autonomous driving and new energy vehicle technologies, where precise and intelligent suspension control is increasingly critical.

2.0 METHODOLOGY

The research explores the design and simulation of an electromagnetic suspension spring intended to enhance vehicle ride comfort and dynamic stability. Compared to traditional passive systems, this electromagnetic suspension offers actively controlled stiffness and damping properties, thus responding adaptively to varying road and driving conditions. The methodology involves the conceptual design of an electromagnetic actuator system, implementation of a Proportional-Integral-Derivative (PID) control strategy, realistic pavement excitation modeling, half-car dynamic modeling, and a comparative analysis between active and passive systems.

2.1 Operating Principle of Electromagnetic Suspension

Building upon the conventional McPherson suspension system, the proposed model integrates an electromagnetic actuator based on the Vehicle Control Module (VCM) principle to form a parallel arrangement with the mechanical spring and damper. This

hybrid structure enables two operational modes with active vibration suppression through PID-controlled electromagnetic force generation and energy recovery mode for regenerative braking, where vibrational energy is stored in the vehicle's battery system. The electromagnetic suspension structure and its working principle are depicted in Figure 1, illustrating the functional components and their integration into the suspension assembly.

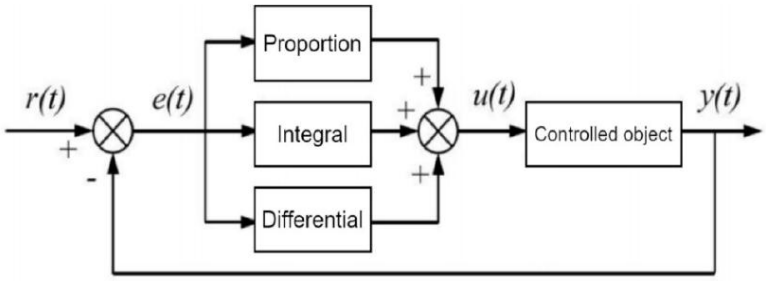

Figure 1: PID control principle diagram

The PID controller operates as a closed-loop system that minimizes the error between a target value and the actual output by processing the deviation through three control actions which are the proportional, integral, and derivative. The proportional term responds to present errors, the integral term eliminates steady-state errors by accumulating past deviations, and the derivative term predicts future error trends, enhancing system stability and responsiveness. Its advantages include simple structure, easy tuning, and adaptability to various applications such as vehicle dynamics. The PID system ensures precise, stable control with low cost and real-time adjustment capability, improving ride comfort and safety under changing road conditions.

2.2 PID Control Strategy Development

The active suspension system was specifically designed to optimize key vehicle dynamic responses, focusing on reducing body acceleration, pitch angular acceleration, and suspension dynamic deflection. Among these, minimizing body acceleration was prioritized as it directly influences ride comfort and overall vehicle performance. The target output of the PID controller was set to ensure near-zero body acceleration, with the electromagnetic force generated by the half-car model's front and rear actuators serving as the control output. The tuning of the PID controller's parameters, Kp (proportional gain), Ki (integral gain), and Kd (derivative gain), was critical to achieving the desired system performance. Table 1 presents the general influence of these parameters on the system responses, showing how each gain affects overshoot, response speed, settling time, and steady-state error.

Table 1. Relationship between control parameters and control effects

Controls Parameter	Respond Speed	Overshoot	Settling Time	Steady-State Error
Kp	Increase	Decrease	Minor Changes	Increase
Ki	Decrease	Increase	Increase	Eliminate
Kd	Minor Changes	Decrease	Decrease	Minor Changes

Though a trial-and-error method, the PID controller parameters were carefully adjusted to achieved optimal suspension performance. The Kp was increased gradually and set at

ISSN 2180-1053 e-ISSN 2289-8123 Vol.17 No.2

37 to ensure a quick system response while preventing excessive oscillations. The Kd was adjusted from zero upwards to reduce oscillation amplitude and improve system stability, with an optimal value of 0.1 being determined to suppress vibrations without delaying system response. Similarly, the Ki was fine-tuned to 0.1 to effectively eliminate steady-state error while maintaining system stability and avoiding additional oscillations. The parameter combination of Kp=37, Ki=0.1, and Kd=0.1 provided the best balance between ride comfort, vibration damping, and pitch angle control. The tuning process was guided by evaluating simulation results to ensure minimal body acceleration and optimal pitch angle stability. The complete structure of the PID control subsystem built in MATLAB/Simulink is shown in Figure 2, illustrating how the error between the references and actual vehicle responses is processed through PID actions to adjust actuator forces accordingly.

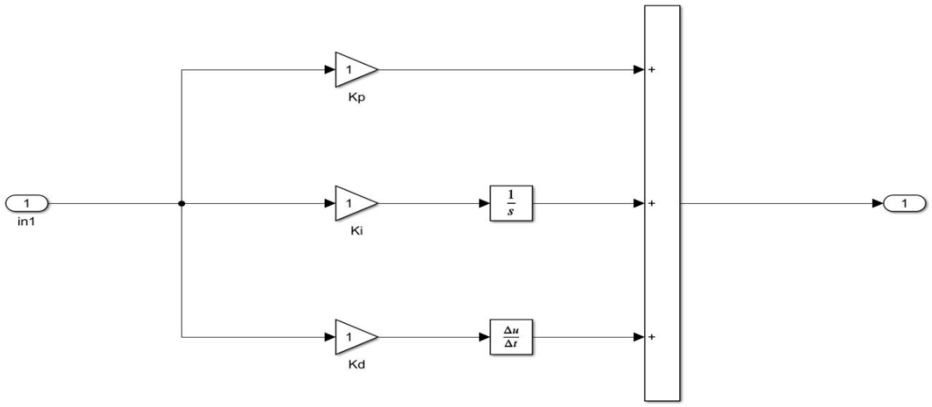

Figure 2: PID control sub-model

2.3 Pavement Excitation Modeling

The pavement excitation serves as one of the most critical sources of vehicle vibration. Here, the vehicle vibration originates from three primary sources. The first is road surface undulations that transmit excitation energy through the tires. The second is vibrations induced by the engine and other powertrain components. The third is disturbances resulting from movements of the driver or passengers inside the vehicle. Among these, road surface roughness has the most significant impact on vehicle vibration levels, especially as the vehicle drives over fluctuating pavement surfaces that introduce considerable excitation energy into the vehicle body.

To accurately replicate real-road excitation in simulation, a time-domain pavement excitation model was established. According to the Chinese National Standard GB/T7031-1986, road surfaces are classified into eight levels of roughness ranging from class A to class H based on their power spectral density (PSD) characteristics. As summarized in Table 2, the majority of domestic roads fall into Class B and Class C categories. In this study, Class C pavement was specifically selected because it represents the typical roughness characteristics of most Chinese roadways. The vehicle's driving speed was set at 40 m/s to simulate highway-level conditions. Since the research adopted a half-vehicle model as the analysis object, the delay between the front and rear wheel excitations was carefully considered. For a vehicle traveling at 40 m/s, the rear wheel experiences a time

delay of 0.32 s relative to the front wheel as both pass over the same road profile. This setting accurately accounts for the wheelbase and speed relationship.

Table 2. Pavement roughness classification

Road Surface Grade	Lower Limit	Geometric Mean	Upper Limit	Lower Limit	Geometric Mean	Upper Limit
A	8	16	32	2.69	3.81	5.38
B	32	64	128	5.28	7.61	10.77
C	128	256	512	10.77	15.23	21.53
D	512	1024	2048	21.53	30.45	43.06
E	2048	4096	8192	73.06	60.90	86.12
F	8192	16384	32768	86.13	121.80	172.26
G	32768	65536	131072	172.26	243.61	344.52
H	131072	262144	524288	344.52	487.22	689.04

The random pavement excitation model based on Class C road roughness was constructed in MATLAB/Simulink. The schematic diagram of the road surface excitation simulation model is shown in Figure 3, which illustrates the generation of random road displacement inputs according to ISO-based PSD data. The corresponding time-domain simulation results of the C-Class pavement excitation input is presented in Figure 4, clearly showing the generated road profile applied to the suspension system. The power spectrum unevenness coefficient of the road surface was $G_q(n_0) = 256 \times 10^{-6}$ m^3, and the vehicle driving speed was set at 40 m/s. Based on the semi-truck model study, there was a delay of 0.032 m for the rear wheels compared to the front wheels when passing the same level of road surface.

This realistic excitation model enabled the detailed analysis of suspension dynamic responses under standard road disturbance conditions. It ensured that the electromagnetic active suspension system's performance evaluation was both accurate and relevant to actual driving scenarios. Based on the fluctuation of the curves in the Figure 4, within the time interval of 0 to 5 s, the road height fluctuated with time, indicating that the road height changes were relatively frequent, meaning that the frequency of road unevenness changes was high. Such high frequency road unevenness changes would have frequent excitation effects on the vehicle's suspension system and driving stability, and in this research project, the influence of this high frequency road input on vehicle performance need to be considered.

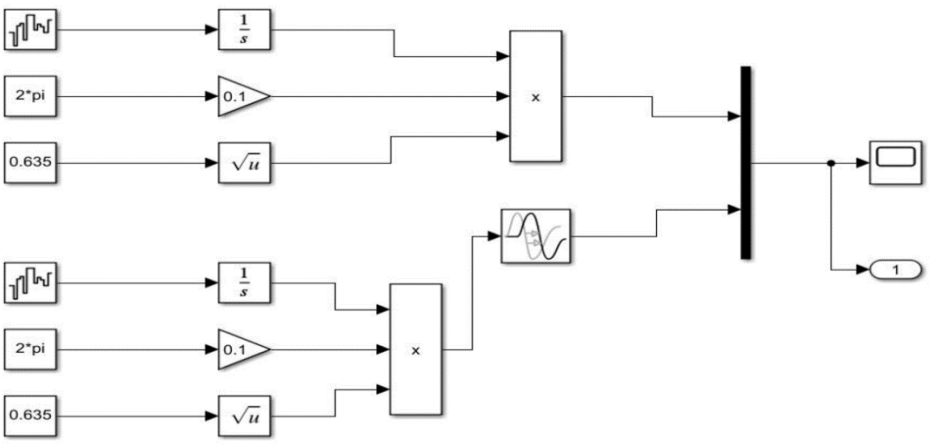

Figure 3: Simulation model of random road surface dynamics

ISSN 2180-1053 e-ISSN 2289-8123 Vol.17 No.2

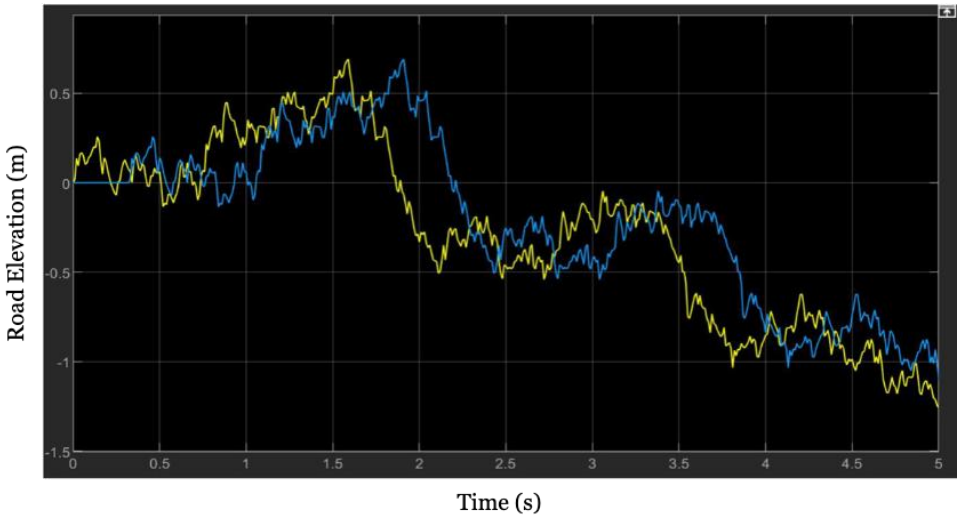

Figure 4: Simulation results of random road input

2.4 Half-Car Suspension System Modeling

To simplify the complexity inherent in vehicle suspension systems while retaining essential dynamic characteristics, a half-car model was established for simulating both passive and electromagnetic active suspension systems. Several modeling assumptions were made to facilitate this simplification. Firstly, the suspension systems were treated as linear spring-damper assemblies. Secondly, the connections between the wheel and the frame were modeled as rigid unsprung masses, while the connection between the body and seating components was modeled as the sprung mass. Additionally, small vibrations around the equilibrium position were assumed when the car body's pitch angle acceleration remained constant. The tire stiffness was considered constant and unaffected by damping characteristics, and the electromagnetic actuator's current coefficient was assumed to remain stable despite magnetic field interactions. These assumptions allowed for a manageable yet sufficiently accurate representation of vehicle dynamics.

The structural and physical parameters used for the half-car model were derived from an experimental prototype, with detailed values provided in Table 3. These parameters were essential inputs for accurately simulating the system's vertical and pitch dynamics under various road excitations. Here, the half-car model was implemented using MATLAB/Simulink to construct both passive and active suspension simulation environments. The passive suspension system model used for random road is illustrated in Figure 5, while the electromagnetic active suspension model equipped with PID control is shown in Figure 6. These simulation models enabled comparative analysis of suspension performance, facilitating evaluation of the electromagnetic suspension's effectiveness in improving vehicle ride comfort, stability, and vibration control compared to the passive system.

Table 3. Structural parameters of experimental prototype

Items	Numerical Value	Unit
Sprung Mass (ms)	2.74	Kg
Moment of Inertia of the Spring-Loaded Mass (Isy)	10.15	$Kg \cdot m^2$
Unsprung Mass of the Front Suspension (Mwf)	5.43	Kg

ISSN 2180-1053 e-ISSN 2289-8123 Vol.17 No.2

Items	Numerical Value	Unit
Unsprung Mass of the Actual Suspension (Mwr)	5.43	Kg
Spring Stiffness of the Front Suspension (Ksf)	3400	N/m
Spring Stiffness of the Rear Suspension (Ksr)	3200	N/m
Damping Coefficient of the Front Suspension (Csf)	5	$N/m \cdot s$
Damping Coefficient of the Real Suspension (Csr)	5	$N/m \cdot s$
Front Suspension Elastic Element Stiffness (Kwf)	2600	N/m
Rear Suspension Elastic Element Stiffness (Kwr)	2600	N/m
Distance (α)	0.18	m
Distance (β)	0.18	m
Wheelbase (L)	0.36	m

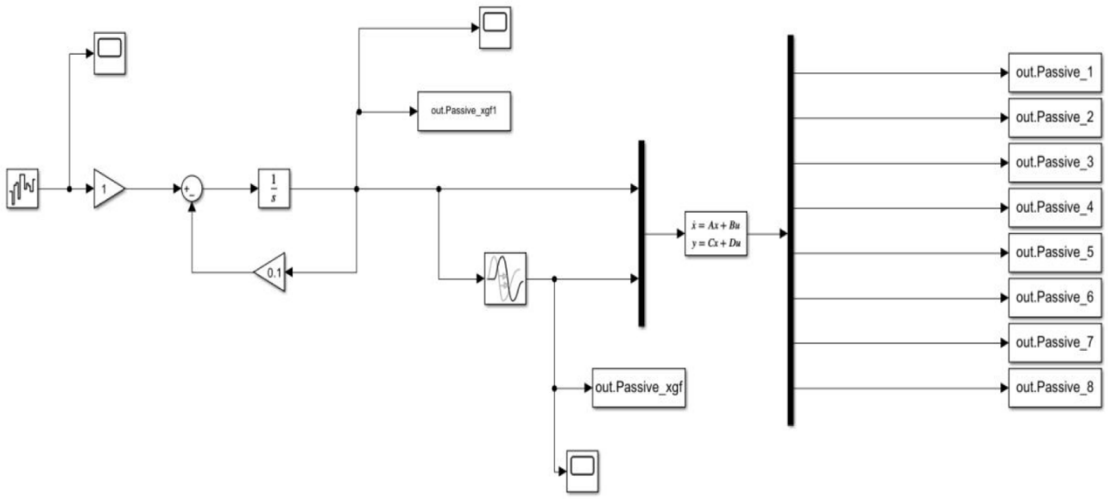

Figure 5: Passive suspension random road simulation diagram

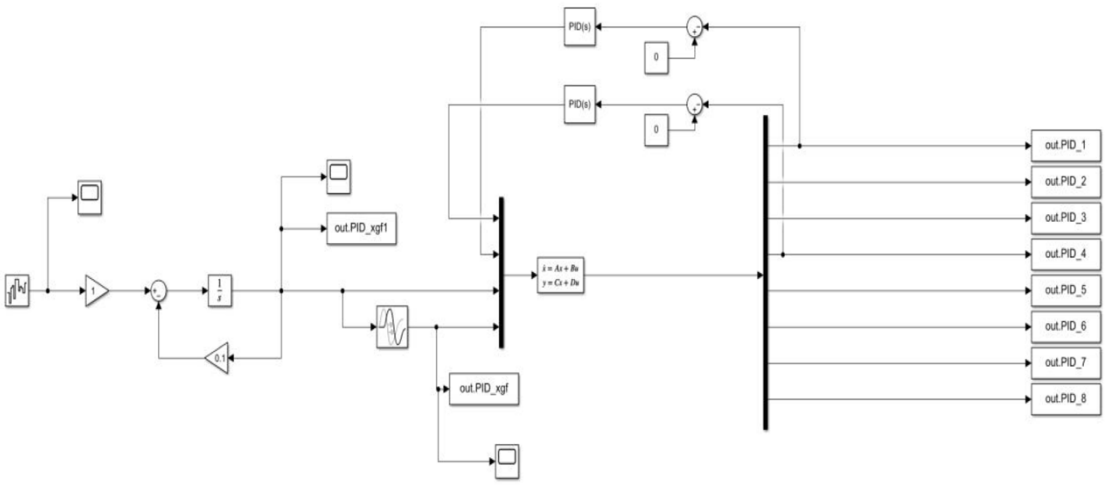

Figure 6: PID control electromagnetic suspension simulation diagram

2.5 Modeling of Half-Car Four-Degree-of-Freedom Passive Suspension System

In order to reflect the improvement of the performance of the electromagnetic active suspension system, it is necessary to first establish the system dynamics model of the passive suspension in MATLAB/Simulink, as well as the system dynamics model of the electromagnetic active suspension under the action of the PID controller. The simplified half-car passive suspension system dynamics model is shown in Figure 7. The suspension

ISSN 2180-1053 e-ISSN 2289-8123 Vol.17 No.2

performance is evaluated by analyzing the longitudinal acceleration of the vehicle's center of mass, the acceleration of the pitch angle, and the dynamic deformation of the front and rear suspensions.

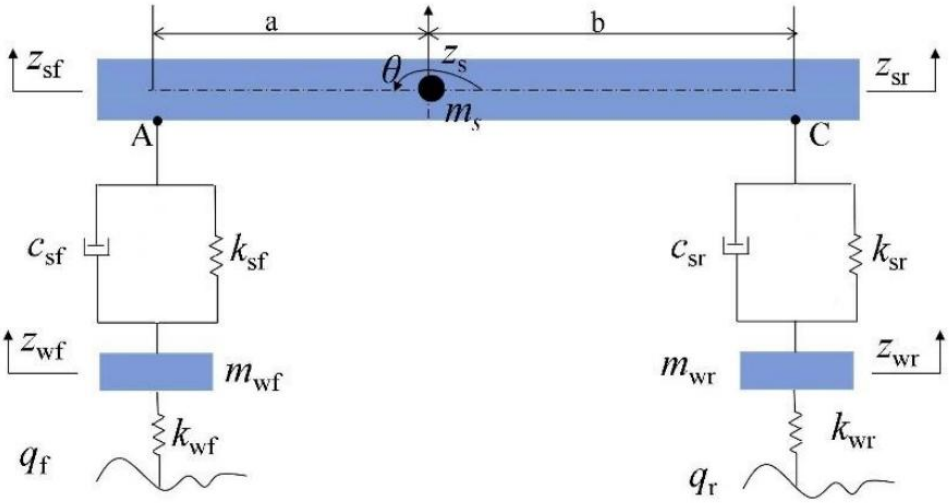

Figure 7: Half-car four-degree-of-freedom passive suspension model

The physical quantities of the half-car four-degree-of-freedom passive suspension are as follows where m_s is the sprung mass, I_{sy} is the moment of inertia of the sprung mass around the suspension center of mass position, m_{wf} and m_{wr} are the unsprung masses on the front and rear suspension wheels, a and b are the lengths between the front and rear wheels and the equivalent center of mass of the suspension, K_{sf} and K_{wf} are the stiffness of front and rear suspension elastic elements respectively, C_{sf} and C_{sr} are the tire stiffness of front and rear suspension wheels, q_f and q_r are the road excitation of front and rear suspension tires respectively. Z_{wf} and Z_{wr} are the longitudinal displacement of the unsprung mass of the front and rear suspension wheels while Z_{sf} and Z_{sr} are the longitudinal displacement of the sprung mass of the front and rear suspension. Z_s is the longitudinal displacement of the equivalent center of mass of the vehicle. If the dynamics model of half-car suspension system can be regarded as a rigidly connected rigid body after simplification, and the variation range of the pitch angle value of the position at the center of mass of the dynamics model is extremely small, which can be expressed as $sin\phi = \phi$, then the equations can be expressed as Equations (1) and (2).

$$Z_{sf} = Z_s - a\phi \tag{1}$$

$$Z_{sr} = Z_s - b\phi \tag{2}$$

With reference to D 'Alembert's principle and with the frame as the research object, the dynamic equations of longitudinal vibration and pitch motion at the equivalent center of mass position of the suspension can be expressed as Equations (3) and (4).

$$m_s\ddot{z}_s = K_{sf}(z_{wf} - z_{sf}) + C_{sf}(\dot{z}_{wf} - \dot{z}_{sf}) + K_{sr}(z_{wr} - z_{sr}) + C_{sf}(\dot{z}_{wr} - \dot{z}_{sr}) \tag{3}$$

$$I_{sy}\ddot{\phi} = bK_{sr}(z_{wr} - z_{sr}) + bC_{sr}(\dot{z}_{wr} - \dot{z}_{sr}) - aK_{sf}(z_{wf} - z_{sf}) - aC_{sf}(\dot{z}_{wf} - \dot{z}_{sf}) \tag{4}$$

ISSN 2180-1053 e-ISSN 2289-8123 Vol.17 No.2

The dynamic equation of the former and post-unsprung masses as the object of study can be expressed as Equations (5) and (6).

$$m_{wf}\ddot{z}_{wf} = K_{wf}\left(z_{qf} - z_{wf}\right) - K_{sf}\left(z_{wf} - z_{sf}\right) - C_{sf}\left(\dot{z}_{wf} - \dot{z}_{sf}\right) \tag{5}$$

$$m_{wr}\ddot{z}_{wr} = K_{wr}\left(z_{qr} - z_{wr}\right) - K_{sr}(z_{wr} - z_{sr}) - C_{sr}(\dot{z}_{wr} - \dot{z}_{sr}) \tag{6}$$

Take the system state space variable is given as Equation (7).

$$X_1 = \left(z_s, \phi, z_{wf}, z_{wr}, \dot{z}_s, \dot{\phi}, \dot{z}_{wf}, \dot{z}_{wr}\right)^{\mathrm{T}} \tag{7}$$

The input variable is given as Equation (8).

$$U = \left(q_f, q_r\right)^{\mathrm{T}} \tag{8}$$

The output variable is given as Equation (9).

$$Y_1 = \left(\ddot{z}_s, \ddot{\phi}, \ddot{z}_{wf}, \ddot{z}_{wr}, z_{swf}, z_{swr}, K_{wf}z_{qwf}, K_{wr}z_{qwr}\right)^{\mathrm{T}} \tag{9}$$

Then its state space expression can be expressed as Equation (10).

$$\begin{cases} \dot{X}_1 = A_1 X + B_1 U \\ Y_1 = C_1 X + D_1 U \end{cases} \tag{10}$$

The matrices A1, B1, C1 and D1 are respectively expressed as Equations (11) to (14).

$$A_I = \begin{bmatrix} 0 & 0 & 0 & 0 & 1 & 0 & 0 & 0 \\ 0 & 0 & 0 & 0 & 0 & 1 & 0 & 0 \\ 0 & 0 & 0 & 0 & 0 & 0 & 1 & 0 \\ 0 & 0 & 0 & 0 & 0 & 0 & 0 & 1 \\ \frac{K_{sf}+K_{sr}}{-m_s} & \frac{aK_{sf}+bK_{sr}}{m_s} & \frac{K_{sf}}{m_s} & \frac{K_{sr}}{m_s} & \frac{C_{sf}+C_{sr}}{-m_s} & \frac{aC_{sf}-bC_{sr}}{m_s} & \frac{C_{sf}}{m_s} & \frac{C_{sr}}{m_s} \\ \frac{aK_{sf}-bK_{sr}}{I_{sy}} & \frac{a^2k_{sf}+b^2K_{sr}}{-I_{sy}} & -\frac{aK_{sf}}{I_{sy}} & \frac{bK_{sr}}{I_{sy}} & \frac{aC_{sf}-bC_{sr}}{I_{sy}} & -\frac{a^2C_{sf}+b^2C_{sr}}{I_{sy}} & \frac{aC_{sf}}{-I_{sy}} & \frac{bC_{sr}}{I_{sy}} \\ \frac{K_{sf}}{m_{wf}} & -\frac{aK_{sf}}{m_{wf}} & \frac{K_{sf}+K_{wf}}{m_{wf}} & 0 & \frac{C_{sf}}{m_{wf}} & -\frac{aC_{sf}}{m_{wf}} & \frac{C_{sf}}{-m_{wf}} & 0 \\ \frac{K_{sr}}{m_{wr}} & \frac{bK_{sr}}{m_{wr}} & 0 & \frac{K_{sr}+K_{wr}}{-m_{wr}} & \frac{C_{sr}}{m_{wr}} & \frac{bC_{sr}}{m_{wr}} & 0 & -\frac{C_{sr}}{m_{wr}} \end{bmatrix} \tag{11}$$

$$B_I = \begin{bmatrix} 0 & 0 \\ 0 & 0 \\ 0 & 0 \\ 0 & 0 \\ 0 & 0 \\ \frac{K_{wf}}{m_{wf}} & 0 \\ 0 & \frac{K_{wr}}{m_{wr}} \end{bmatrix} \tag{12}$$

$$C_1 = \begin{bmatrix} \frac{K_{sf}+K_{sr}}{-m_s} & \frac{aK_{sf}-bK_{sr}}{m_s} & \frac{K_{sf}}{m_s} & \frac{K_{sr}}{m_s} & \frac{C_{sf}+C_{sr}}{-m_s} & \frac{aC_{sf}-bC_{sr}}{m_s} & \frac{C_{sf}}{m_s} & \frac{C_{sr}}{m_s} \\ \frac{aK_{sf}-bK_{sr}}{I_{sy}} & \frac{a^2K_{sf}+b^2K_{sr}}{I_{sy}} & -\frac{aK_{sf}}{I_{sy}} & \frac{bK_{sr}}{I_{sy}} & \frac{aC_{sf}-bC_{sr}}{I_{sy}} & \frac{a^2C_{sf}+b^2C_{sr}}{-I_{sy}} & \frac{aC_{sf}}{-I_{sy}} & \frac{bC_{sr}}{I_{sy}} \\ \frac{K_{sf}}{m_{wf}} & -\frac{aK_{sf}}{m_{wf}} & \frac{K_{sf}+K_{wf}}{-m_{wf}} & 0 & \frac{C_{sf}}{m_{wf}} & \frac{-aC_{sf}}{m_{wf}} & \frac{C_{sf}}{-m_{wf}} & 0 \\ \frac{K_{sr}}{m_{wr}} & \frac{bK_{sr}}{m_{wr}} & 0 & \frac{K_{sr}+K_{wr}}{-m_{wr}} & \frac{C_{sr}}{m_{wr}} & \frac{bC_{sr}}{m_{wr}} & 0 & \frac{-C_{sr}}{m_{wr}} \\ 1 & -a & -1 & 0 & 0 & 0 & 0 & 0 \\ 1 & b & -1 & 0 & 0 & 0 & 0 & 0 \\ 0 & 0 & -K_{wf} & 0 & 0 & 0 & 0 & 0 \\ 0 & 0 & 0 & -K_{wr} & 0 & 0 & 0 & 0 \end{bmatrix} \quad (13)$$

$$D_1 = \begin{bmatrix} 0 & 0 \\ 0 & 0 \\ \frac{K_{wf}}{m_{wf}} & 0 \\ 0 & \frac{K_{wr}}{m_{wr}} \\ 0 & 0 \\ 0 & 0 \\ K_{wf} & 0 \\ 0 & K_{wr} \end{bmatrix} \quad (14)$$

2.6 Modeling of Half-Car Four-Degree-of-Freedom Electromagnetic Active Suspension System

On the basis of the original passive suspension system, electromagnetic active suspension actuators are embedded between the front and rear dampers and springs respectively, and the main power F_{ur} generated, As shown in Figure 8, the electromagnetic drive of F_{ur} is in parallel with the damper and spring, and the body mass of each wheel is combined into a centroid mass m_s. The pitching characteristics of half-car are analyzed through a four-degree-of-freedom mechanical model.

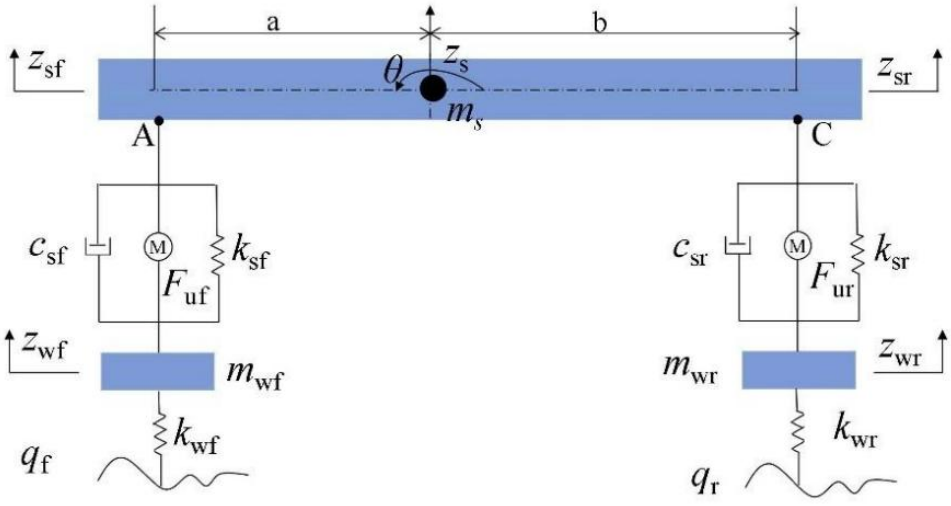

Figure 8. Half-car four-degree-of-freedom electromagnetic active suspension model

Taking the body and the front and rear wheels as the research objects, the system dynamics equation obtained from the force balance and torque balance can be expressed as Equations (15) to (18).

$$m_s\ddot{z}_s = K_{sf}(z_{wf} - z_{sf}) + C_{sf}(\dot{z}_{wf} - \dot{z}_{sf}) + K_{sr}(z_{wr} - z_{sr}) + C_{sr}(\dot{z}_{wr} - \dot{z}_{sr}) + K_{uf}I_f + K_{ur}I_r \tag{15}$$

$$I_{sy}\ddot{\phi} = bK_{sr}(z_{wr} - z_{sr}) + bC_{sr}(\dot{z}_{wr} - \dot{z}_{sr}) - aK_{sf}(z_{wf} - z_{sf}) - aC_{sf}(\dot{z}_{wf} - \dot{z}_{sf}) + bK_{ur}I_r - aK_{uf}I_f \tag{16}$$

$$m_{wf}\ddot{z}_{wf} = K_{wf}(z_{qf} - z_{wf}) - K_{sf}(z_{wf} - z_{sf}) - C_{sf}(\dot{z}_{wf} - \dot{z}_{sf}) - K_{uf}I_f \tag{17}$$

$$m_{wr}\ddot{z}_{wr} = K_{wr}(z_{qr} - z_{wr}) - K_{sr}(z_{wr} - z_{sr}) - C_{sr}(\dot{z}_{wr} - \dot{z}_{sr}) - K_{ur}I_r \tag{18}$$

Take the system state space variable as Equation (19).

$$X_2 = \left(z_s, \phi, z_{wf}, z_{wr}, \dot{z}_s, \dot{\phi}, \dot{z}_{wf}, \dot{z}_{wr}\right)^{\mathrm{T}} \tag{19}$$

The input variable is given as Equation (20).

$$U = \left(I_f, I_r, q_f, q_r\right)^{\mathrm{T}} \tag{20}$$

The output variable is given as Equation (21).

$$Y_2 = \left(\ddot{z}_s, \ddot{\phi}, \ddot{z}_{wf}, \ddot{z}_{wr}, z_{swf}, z_{swr}, K_{wf}z_{qwf}, K_{wr}z_{qwr}\right)^{\mathrm{T}} \tag{21}$$

Then its state space expression can be expressed as Equation (22).

$$\begin{cases}\dot{X}_2 = A_2X + B_2U \\ Y_2 = C_2X + D_2U\end{cases} \tag{22}$$

The matrix A2, B2, C2 and D2 are respectively expressed as Equations (24) to (26).

$$A_2 = \begin{bmatrix} 0 & 0 & 0 & 0 & 1 & 0 & 0 & 0 \\ 0 & 0 & 0 & 0 & 0 & 1 & 0 & 0 \\ 0 & 0 & 0 & 0 & 0 & 0 & 1 & 0 \\ 0 & 0 & 0 & 0 & 0 & 0 & 0 & 1 \\ \frac{K_{sf}+K_{sr}}{-m_s} & \frac{aK_{sf}-bK_{sr}}{m_s} & \frac{K_{sf}}{m_s} & \frac{K_{sr}}{m_s} & -\frac{C_{sf}+C_{sr}}{m_s} & \frac{aC_{sf}-bC_{sr}}{m_s} & \frac{C_{sf}}{m_s} & \frac{C_{sr}}{m_s} \\ \frac{aK_{sf}-bK_{sr}}{I_{sy}} & \frac{a^2K_{sf}+b^2K_{sr}}{-I_{sy}} & -\frac{aK_{sf}}{I_{sy}} & \frac{bK_{sr}}{I_{sy}} & \frac{aC_{sf}-bC_{sr}}{I_{sy}} & \frac{a^2C_{sf}+b^2C_{sr}}{-I_{sy}} & -\frac{aC_{sf}}{I_{sy}} & \frac{bC_{sr}}{I_{sy}} \\ \frac{K_{sf}}{m_{wf}} & -\frac{aK_{sf}}{m_{wf}} & \frac{K_{sf}+K_{wf}}{-m_{wf}} & 0 & \frac{C_{sf}}{m_{wf}} & -\frac{aC_{sf}}{m_{wf}} & \frac{C_{sf}}{-m_{wf}} & 0 \\ \frac{K_{sr}}{m_{wr}} & \frac{bK_{sr}}{m_{wr}} & 0 & \frac{K_{sr}+K_{wr}}{-m_{wr}} & \frac{C_{sr}}{m_{wr}} & \frac{bC_{sr}}{m_{wr}} & 0 & \frac{C_{sr}}{-m_{wr}} \end{bmatrix} \tag{23}$$

ISSN 2180-1053 e-ISSN 2289-8123 Vol.17 No.2

$$B_2 = \begin{bmatrix} 0 & 0 & 0 & 0 \\ 0 & 0 & 0 & 0 \\ 0 & 0 & 0 & 0 \\ 0 & 0 & 0 & 0 \\ \frac{K_{uf}}{m_s} & \frac{K_{ur}}{m_s} & 0 & 0 \\ -\frac{aK_{uf}}{I_{sy}} & \frac{bK_{ur}}{I_{sy}} & 0 & 0 \\ -\frac{K_{uf}}{m_{wf}} & 0 & \frac{K_{wf}}{m_{wf}} & 0 \\ 0 & -\frac{K_{ur}}{m_{wr}} & 0 & \frac{K_{wr}}{m_{wr}} \end{bmatrix} \quad (24)$$

$$C_2 = \begin{bmatrix} \frac{K_{sf}+K_{sr}}{-m_s} & \frac{aK_{sf}-bK_{sr}}{m_s} & \frac{K_{sf}}{m_s} & \frac{K_{sr}}{m_s} & -\frac{C_{sf}+C_{sr}}{m_s} & \frac{aC_{sf}-bC_{sr}}{m_s} & \frac{C_{sf}}{m_s} & \frac{C_{sr}}{m_s} \\ \frac{aK_{sf}-bK_{sr}}{I_{sy}} & \frac{a^2K_{sf}+b^2K_{sr}}{-I_{sy}} & -\frac{aK_{sf}}{I_{sy}} & \frac{bK_{sr}}{I_{sy}} & \frac{aC_{sf}-bC_{sr}}{I_{sy}} & \frac{a^2C_{sf}+b^2C_{sr}}{-I_{sy}} & -\frac{aC_{sf}}{I_{sy}} & \frac{bC_{sr}}{I_{sy}} \\ \frac{K_{sf}}{m_{wf}} & -\frac{aK_{sf}}{m_{wf}} & \frac{K_{sf}+K_{wf}}{-m_{wf}} & 0 & \frac{C_{sf}}{m_{wf}} & -\frac{aC_{sf}}{m_{wf}} & \frac{C_{sf}}{-m_{wf}} & 0 \\ \frac{K_{sr}}{m_{wr}} & \frac{bK_{sr}}{m_{wr}} & 0 & \frac{K_{sr}+K_{wr}}{-m_{wr}} & \frac{C_{sr}}{m_{wr}} & \frac{bC_{sr}}{m_{wr}} & 0 & \frac{C_{sr}}{-m_{wr}} \\ 1 & -a & -1 & 0 & 0 & 0 & 0 & 0 \\ 1 & b & -1 & 0 & 0 & 0 & 0 & 0 \\ 0 & 0 & -K_{wf} & 0 & 0 & 0 & 0 & 0 \\ 0 & 0 & 0 & -K_{wr} & 0 & 0 & 0 & 0 \end{bmatrix} \quad (25)$$

$$D_2 = \begin{bmatrix} 0 & 0 & \frac{K_{uf}}{m_s} & \frac{K_{ur}}{m_s} \\ 0 & 0 & -\frac{aK_{uf}}{I_{sy}} & \frac{bK_{ur}}{I_{sy}} \\ \frac{K_{wf}}{m_{wf}} & 0 & -\frac{K_{uf}}{m_{wf}} & 0 \\ 0 & \frac{K_{wr}}{m_{wr}} & 0 & -\frac{K_{ur}}{m_{wr}} \\ 0 & 0 & 0 & 0 \\ K_{wf} & 0 & 0 & 0 \\ 0 & K_{wr} & 0 & 0 \\ 0 & 0 & 0 & K_{wr} \end{bmatrix} \quad (26)$$

3.0 RESULTS AND DISCUSSION

This research project used MATLAB and Simulink software to compare the performance of the electromagnetic active suspension system controlled by a PID strategy with that of a traditional McPherson suspension. The study focused on four aspects of vehicle body acceleration, pitch angle acceleration, front suspension dynamic travel and rear suspension dynamic travel. The PID control system was tuned with parameters Kp equal

ISSN 2180-1053 e-ISSN 2289-8123 Vol.17 No.2

to 37, Ki equal to 0.1 and Kd equal to 0.1. The PID parameters used in this study were obtained through a systematic trial-and-error tuning process to ensure an effective balance between stability, response speed, and vibration suppression. The Kp was first adjusted by gradually increasing its value from a lower baseline. As Kp increased, the system response became faster, however, higher values also introduced oscillations. At Kp = 37, the suspension system achieved an appropriate compromise, providing quick response while avoiding excessive instability or overshoot.

Following the adjustment of Kp, the Kd was tuned to further improve system stability. Beginning with Kd = 0, the system exhibited oscillations at Kp = 37. Incremental increases in Kd allowed these oscillations to be damped effectively while maintaining a sufficiently rapid transient response. The value of Kd = 0.1 was found to provide the best balance, significantly reducing vibration without introducing delay in the system's response.

Finally, the Ki was adjusted to address steady-state error in the system response. With Kp = 37 and Kd = 0.1 fixed, the system exhibited small residual errors in reaching the target value. By gradually increasing Ki, the steady-state error was eliminated while ensuring that no additional oscillations were introduced. A value of Ki = 0.1 was determined to provide accurate target tracking while preserving overall system stability.

The chosen PID parameters therefore represent the optimal values for this research. In this context, "optimum" performance is defined according to three main criteria of minimizing oscillations during transient responses, maintaining a rapid and stable response to road disturbances, and eliminating steady-state error while keeping vibration levels within comfort and safety limits.

These criteria, aligned with the suspension performance objectives of ride comfort, stability, and effective vibration suppression, form the standard by which the parameter values were verified and selected. The simulation aimed to quantify improvements in ride comfort and stability by measuring root mean square and peak values across each dynamic response indicator. By examining how real-time adjustment of damping and stiffness affects vibrations transmission and suspension travel, the study provides evidence for the effectiveness of electromagnetic active suspension in enhancing driving quality under identical road conditions.

3.1 Automobile Body Acceleration Simulation Analysis

The simulation results show a clear reduction in vehicle body acceleration when using the electromagnetic active suspension system compared to the passive McPherson design as shown in Figure 9. Specifically, the root mean square value of body acceleration was reduced from 6.6994 m/s^2 in the passive suspension to 4.8308 m/s^2 with PID-controlled active suspension, reflecting a performance improvement of approximately 27%. Peak body acceleration also decreased, indicating fewer abrupt movements that passengers can feel inside the cabin.

Further analysis of the time-domain results highlights two key observations as shown in Figure 10. At the 3-second mark, the PID -controlled electromagnetic suspension

ISSN 2180-1053 e-ISSN 2289-8123 Vol.17 No.2

significantly reduces body acceleration to 5.57 m/s^2, compared with 12.45 m/s^2 for the passive McPherson suspension, demonstrating superior transient response to road disturbances. Additionally, at the 9-second mark where peak acceleration occurs, the active suspension still maintains lower acceleration of 15.70 m/s^2 versus 22.45 m/s^2, indicating its effectiveness in limiting large vibrations and enhancing ride comfort.

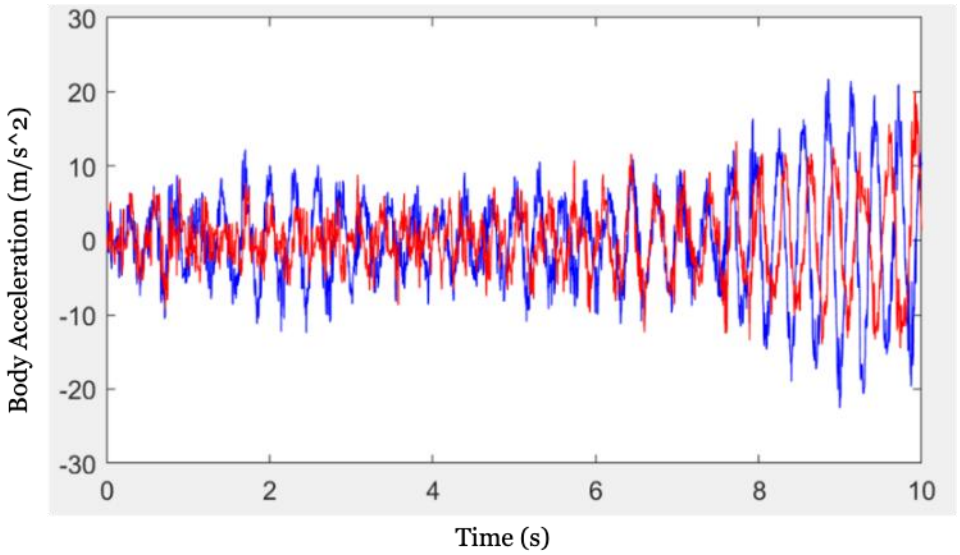

Figure 9: Body acceleration simulation comparison with red for PID-controlled suspension RMS and blue for McPherson suspension RMS

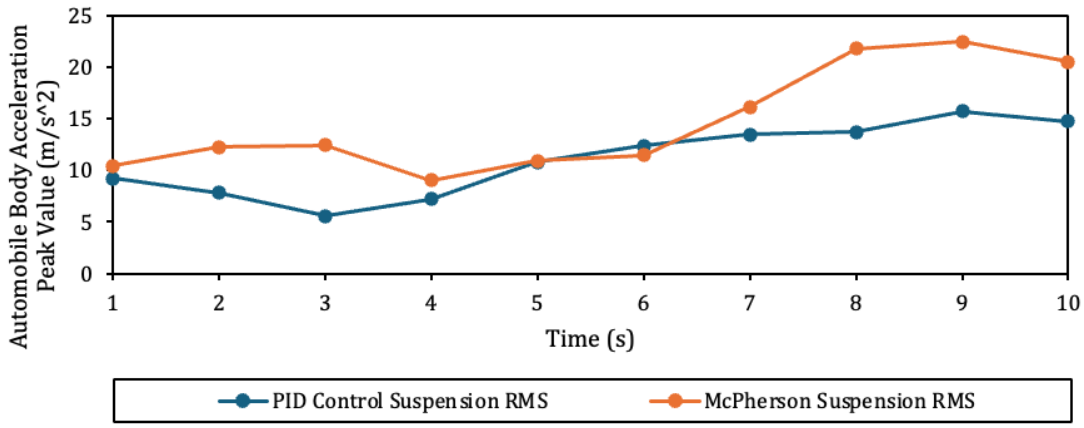

Figure 10: Automobile body acceleration peak value versus time

These reductions suggest that the electromagnetic suspension effectively filters road disturbances by dynamically adjusting damping forces. As the PIC controller responds to changes in road conditions, it modifies suspension stiffness and damping in real time to maintain more stable vehicle body movement. This leads to improved comfort for occupants and helps reduce the risk of resonance effects that can affect vehicle components and passenger experience. The simulation confirms that under identical road inputs, active suspension systems can deliver a smoother ride and improved safety by better controlling vibration transmitted to the vehicle body.

ISSN 2180-1053 e-ISSN 2289-8123 Vol.17 No.2

3.2 Pitch Angle Acceleration Simulation Analysis

Pitch angle acceleration as shown in Figure 11 represents the rotational movement of the vehicle around its lateral axis, often noticeable during acceleration, braking and over uneven road surfaces. The root mean square value of pitch angle acceleration was reduced from 15.1652 rad/s^2 with passive suspension to 11.7992 rad/s^2 using the electromagnetic active suspension, marking an improvement of about 22%. Peak pitch angle acceleration also decreased, further demonstrating the system's effectiveness in reducing sudden body tilting.

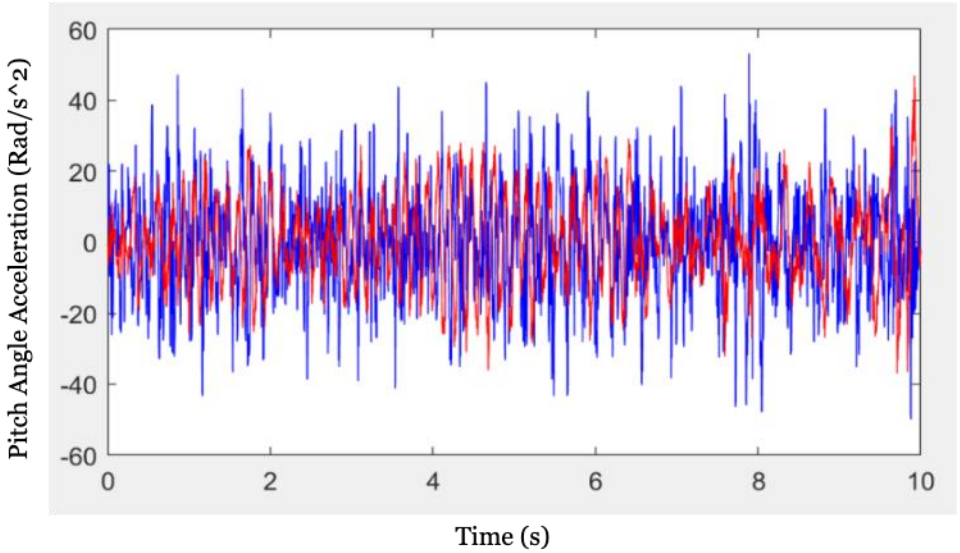

Figure 11: Pitch angle acceleration simulation comparison with red for PID-controlled suspension RMS and blue for McPherson suspension RMS

The time-domain pitch angle acceleration data analysis as shown in Figure 12 reveals two important observations. At the 3-second mark, the PID-controlled electromagnetic suspension significantly reduces pitch acceleration to 16.82 rad/s^2, compared with 38.41 rad/s^2 for the passive suspension, demonstrating a clear advantage in handling sudden disturbances. Additionally, even at the 8-second mark, where both systems experience larger peaks, the active suspension maintains a lower acceleration of 32.19 rad/s^2 versus 52.26 rad/s^2, showing its ability to effectively limit excessive pitch motions under challenging conditions.

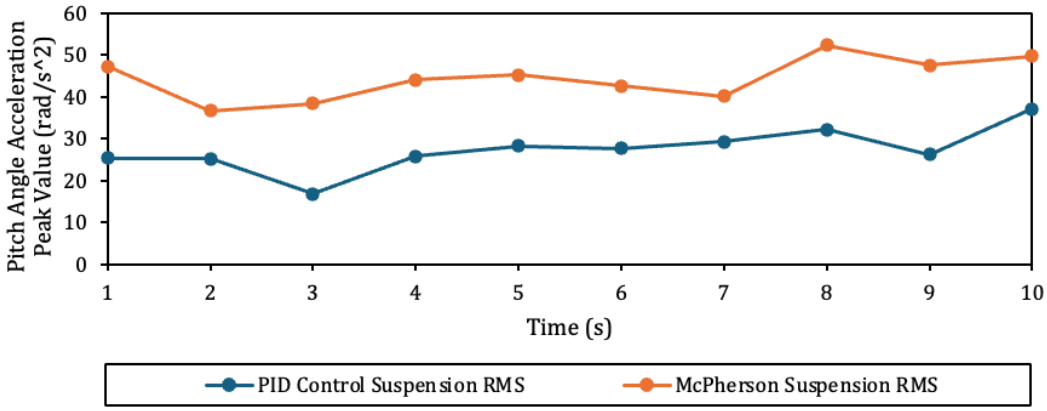

Figure 12: Pitch angle acceleration peak value versus time

ISSN 2180-1053 e-ISSN 2289-8123 Vol.17 No.2

These results highlight how real-time control of stiffness and damping helps limit abrupt pitch movements that affect passenger comfort and vehicle stability. By quickly adapting to external disturbances, the electromagnetic suspension system suppresses excessive body tilt under braking or acceleration, keeping the vehicle posture balanced. In contrast, the passive McPherson suspension cannot adjust dynamically, leading to larger pitch oscillations that can affect driving safety and comfort. This demonstrates that integrating control strategies with electromagnetic suspension technology enhances the dynamic responses and provides a more composed driving experience.

3.3 Simulation Analysis of Front Suspension Dynamic Travel

Front suspension dynamic travel projected in Figure 13 reflects the vertical displacement of the suspension during driving and directly influences handling and comfort. The simulation results show that the electromagnetic active suspension achieved a root mean square dynamic travel of 0.2749 mm, compared to 0.3320 mm for the passive suspension, corresponding to an improvement of about 17%. Peak travel was also reduced, which helps prevent excessive suspension movement that could lead to loss of contact between the tires and road surface.

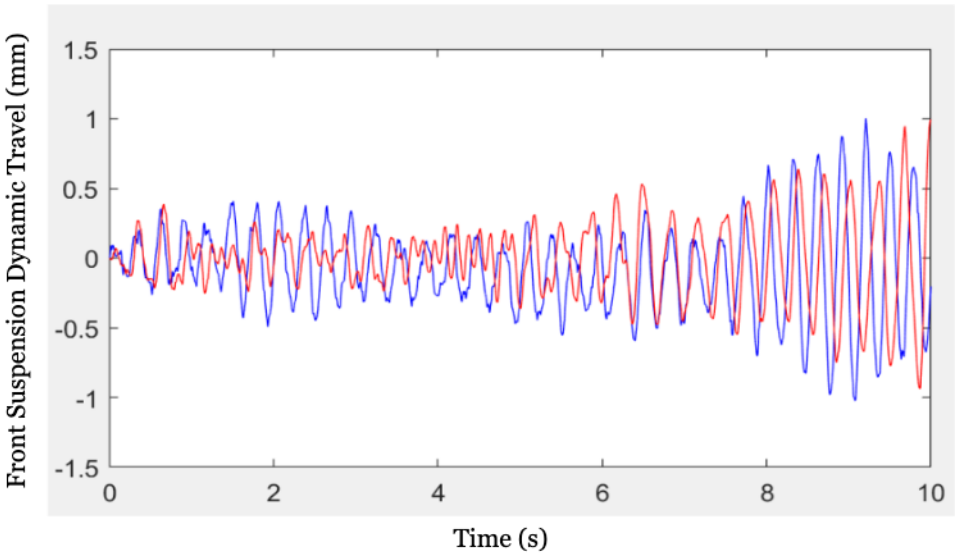

Figure 13: Front suspension dynamic travel simulation comparison with red for PID-controlled suspension RMS and blue for McPherson suspension RMS

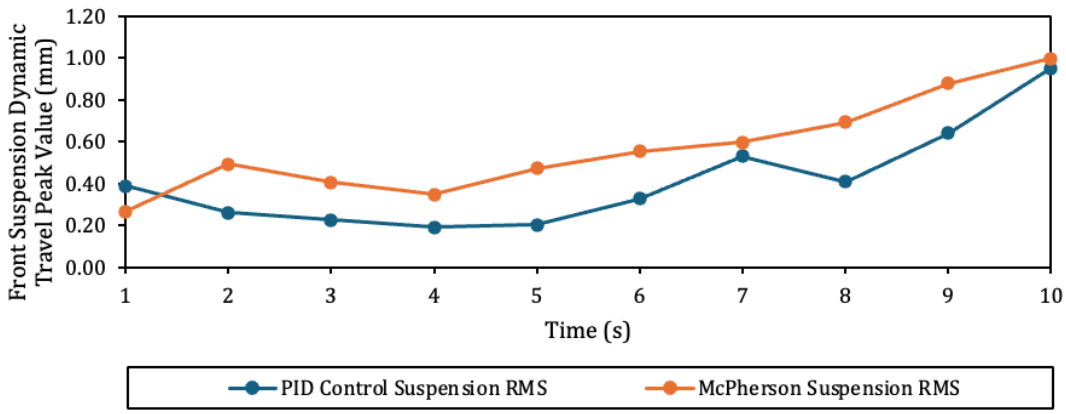

Figure 14: Front suspension dynamic travel peak value versus time

ISSN 2180-1053 e-ISSN 2289-8123 Vol.17 No.2

The time-domain results provided in Figure 14 show that the PID-controlled electromagnetic suspension maintains lower dynamic travel values than the passive suspension throughout simulation. Across the entire period, the active system's peak dynamic travel stays around 0.95 mm, slightly lower than the passive suspension peak of about 1.00 mm.

More importantly, for most of the simulation, the active suspension keeps dynamic travel between roughly 0.19 mm and 0.64 mm, while the passive system ranges higher, from about 0.26 mm to nearly 0.88 mm. This reduction in both average and peak values confirms that real-time adjustment of damping and stiffness effectively limits excessive vertical movement, improves road holding, and enhances overall ride comfort and handling stability.

By adjusting damping and stiffness in real time, the electromagnetic suspension limits large vertical movements in the front wheels. This stabilizes the tire-road contact patch and helps maintain steering precision, especially when driving over uneven surfaces. Lower suspension travel reduces the potential for bottoming out and lessens wear on suspension components. The data demonstrate that this dynamic adaptability improves both ride quality and vehicle handling without compromising the suspension system's ability to absorb road irregularities.

3.4 Simulation Analysis of Dynamic Travel of the Rear Suspension

The rear suspension plays a critical role in balancing body stability, particularly during acceleration and on rough roads. The simulation provided in Figure 15 shows that the electromagnetic active suspension system reduced the root mean square dynamic travel from 0.2926 mm in the passive suspension to 0.1683 mm, an improvement of approximately 42.4%. Peak rear suspension travel was similarly reduced, which is significant for controlling rear axle motion and maintaining passenger comfort in the back seats.

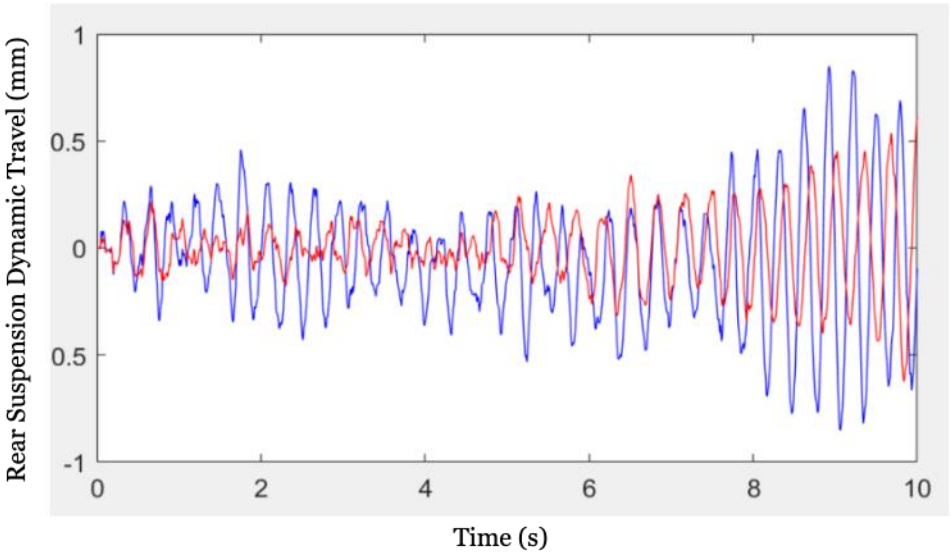

Figure 15: Rear suspension dynamic travel simulation comparison with red for PID-controlled suspension RMS and blue for McPherson suspension RMS

ISSN 2180-1053 e-ISSN 2289-8123 Vol.17 No.2

Examination of the time-domain data as shown in Figure 16 reveals that the PID-controlled electromagnetic suspension consistently keeps rear suspension dynamic travel at lower levels than the passive system. While the passive suspension shows higher fluctuations, often exceeding 0.50 mm and peeking near 0.85 mm, the active system generally holds dynamic travel below 0.45 mm, with a peak of around 0.62 mm. This trend demonstrates that active control smooths out larger displacements, especially under sudden road inputs, and prevents excessive vertical motion of the rear axle.

Through continuous monitoring of road inputs and adjusting damping and stiffness, the electromagnetic suspension effectively limits large vertical displacements at the rear wheels. This helps keep the vehicle body more stable and reduces the oscillations that passengers feel, lowering fatigue and improving ride quality. In contrast, the passive suspension relies on fixed characteristics and cannot react to changing loads, leading to large suspension strokes and less predictable dynamic behavior. The simulation confirms that an actively controlled suspension can better adapt to road conditions, improve comfort and enhance driving safety by maintaining stable rear axle dynamics.

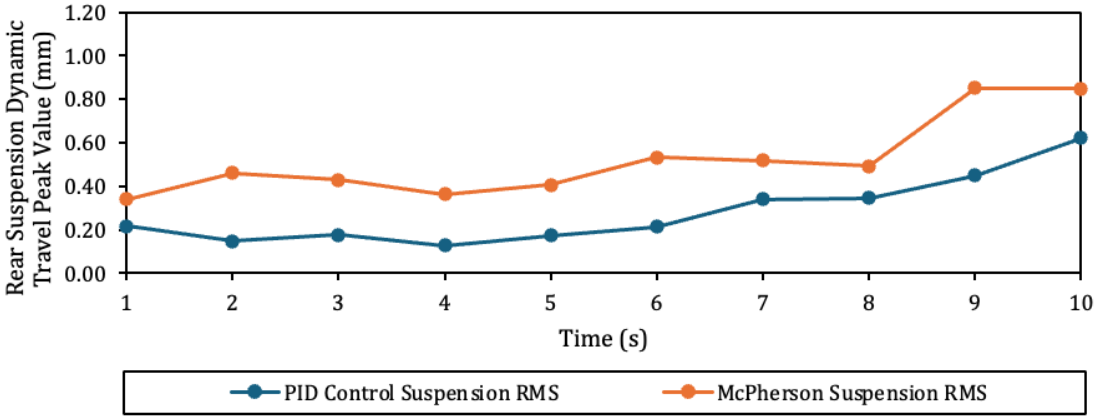

Figure 16: Rear suspension dynamic travel peak value versus time

3.5 Comparative Simulation Results

The final simulation comparison between the electromagnetic active suspension with PID control and the conventional passive McPherson suspension demonstrates significant improvements in dynamic performance across multiple aspects. The active suspension reduced body acceleration by approximately 27% and pitch angle acceleration by around 22%, effectively lowering the vibration levels experienced by passengers and enhancing ride comfort. In terms of suspension travel, the system achieved a reduction of about 17% at the front and an even more pronounced improvements of over 42% at the rear, which helps maintain tire-road contact and limits excessive body motion. These improvements reflect the ability of the PID-controlled electromagnetic suspension to dynamically adjust damping and stiffness in response to varying road conditions, resulting in smoother vehicle responses and better handling stability. Collectively, the data confirm that active control, strategies can bring measurable benefits over passive designs, supporting the goal of achieving higher levels of safety, comfort and driving quality in modem automotive engineering.

ISSN 2180-1053 e-ISSN 2289-8123 Vol.17 No.2

4.0 CONCLUSION

This research proposed and simulated an electromagnetic active suspension system built on the traditional McPherson suspension architecture, integrating a PID control strategy to achieve real-time adjustment of damping and stiffness. Through modeling and analysis, the system was tested across four performance aspects of body acceleration, pitch angle acceleration, front suspension dynamic travel, and rear suspension dynamic travel. Simulation results demonstrated measurable improvements, with reductions in vibration and suspension movement ranging from approximately 17% to over 42% compared to the passive design. These improvements validate that electromagnetic actuation combined with PID control can effectively filter road disturbances and maintain better tire-road contact, thereby enhancing ride f=comfort and handling stability. The PID parameters were verified through a systematic tuning process, where Kp, Ki, and Kd were gradually adjusted to balance rise time, stability, oscillation suppression, and steady-state accuracy. The final values (Kp = 37, Ki = 0.1, Kd = 0.1) were selected as the optimum set according to criteria of rapid and stable response, minimal oscillations, and elimination of steady-state error. It should also be noted that the McPherson suspension model applied in this study was based on experimental teaching equipment at our institution. While this provided a consistent baseline for comparing passive and active suspension performance under identical conditions, its parameters may differ from those of actual vehicle suspension. As such, direct validation against real vehicle data or published experimental results has not yet been performed. Future work will focus on conducting such validation to further confirm the generalizability and practical applicability of the findings. Overall, the study demonstrates that integrating active control strategies into existing suspension layouts can deliver significant improvements in comfort, stability, and safety, while also offering a feasible pathway for advancing modern automotive suspension design.

ACKNOWLEDGEMENT

The authors would like to thank the Department of Aerospace Engineering, Faculty of Engineering, University Putra Malaysia, for their academic and technical guidance throughout this research. The authors are also grateful to the School of Automotive Engineering, Dongying Vocational College of Science and Technology, for providing administrative support and computational resources. In addition, the authors acknowledge the Faculty of Engineering, City University Malaysia, for their academic guidance during the study.

REFERENCES

[1] H. He, Y. Li, J. Z Jiang, S. Burrow, S. Neild, & A. Conn. "Enhancing the trade-off between ride comfort and active actuation requirements via an inerter-based passive-active-combined automotive suspension". *Vehicle System Dynamics, 62*(3), 556–579, 2024.

[2] S.Y. Zhixian. *Effects on vehicle ride comfort of an adaptive suspension system using neural networks* (Master's thesis, University of Windsor, Canada), 2022.

[3] A. Qin, B. Zhang, D. Ning, B. Tan, & H. Du. "A self-sensing approach for estimating suspension displacement and velocity in semi-active electromagnetic dampers". *Mechanical Systems and Signal Processing, 208*, 111049, 2024.

[4] M. Bednarek, D. Lewandowski, K. Polczyński, & J. Awrejcewicz. "On the active damping of vibrations using electromagnetic spring". *Mechanics Based Design of Structures and Machines, 49*(8), 1131–1144, 2021.

[5] B. L. Gysen, J. L. Janssen, J. J. Paulides, & E. A. Lomonova. "Design aspects of an active electromagnetic suspension system for automotive applications". *IEEE Transactions on Industry Applications, 45*(5), 1589–1597, 2009.

[6] E. Asadi, R. Ribeiro, M. B. Khamesee, & A. Khajepour. "A new adaptive hybrid electromagnetic damper: Modelling, optimization, and experiment". *Smart Materials and Structures, 24*(7), 075003, 2015.

[7] X. Xiao, M. Peng, & J. Zou. "Research on factors affecting suspension feed energy potential of commercial vehicles". *Chinese Journal of Highway, 29*(5), 151–158, 2016.

[8] C. Xing, L. Hong, & Z. Deng. "Design and energy-fed analysis of linear motor energy-fed suspension control systems". *Vibration and Shock, 31*(8), 124–129, 2012.

[9] L. Zuo, B. Scully, J. Shestani, J., & Y. Zhou. "Design and characterization of an electromagnetic energy harvester for vehicle suspensions". *Smart Materials and Structures, 19*(4), 045003, 2010.

[10] B. Scully, L. Zuo, J. Shestani, & Y. Zhou. Design and characterization of an electromagnetic energy harvester for vehicle suspensions. *ASME International Mechanical Engineering Congress and Exposition* (Vol. 43833, pp. 1007–1016), 2009.

[11] K. Ding, Y. F. Gu, & G. Q. Zhang. Design of cylinder type transverse flux linear motor actuator for active suspension. *Automobile Applied Technology, 46*(4), 68–71, 2021.

[12] V. R. Prajwal, C. B. Murthy, & , S. D. Yashwanth. Modified electromagnetic actuator for active suspension system. *International Journal of Engineering and Management Research, 11*(4), 188–193, 2021.

[13] X. H. Pu, J. Xu, S. Y. Li, & X. S. Mei. "Effects of inertial mass of electromagnetic damper on vibration insulation performance of vehicle regenerative suspension". *Journal of Xi'an Jiaotong University, 53*(6), 62–68, 2019.

[14] L. Xie, J. Li, X. Li, L. Huang, & S. Cai. "Damping-tunable energy-harvesting vehicle damper with multiple controlled generators: Design, modeling and experiments". *Mechanical Systems and Signal Processing, 99*, 859–872, 2018.

[15] Y. Zhang, H. Chen, K. Guo, X. Zhang, & S.E. Li. "Electro-hydraulic damper for energy harvesting suspension: Modeling, prototyping and experimental validation". *Applied Energy, 199*, 1–12, 2017.

[16] S. A., Chen, X. Li, L. J. Zhao, Y. X. Wang, & Y. B. Kim. "Development of a control method for an electromagnetic semi-active suspension reclaiming energy with varying charge voltage in steps". *International Journal of Automotive Technology, 16*, 765–773, 2015.

[17] H. N .Gao et al. "On-line control method of suspension vibration energy recovery for new energy vehicles". *Journal of Xi'an Jiaotong University, 54*(4), 19–26, 2020.

[18] T. Darabseh, D. Al-Yafeai, A. H. I. Mourad, &F. Almaskari. "Piezoelectric method-based harvested energy evaluation from car suspension system: Simulation and experimental study". *Energy Science & Engineering, 9*(3), 417–433, 2021.

[19] H. F. Yan, & Y.L. Yan. "Design of automotive active suspension system and simulation for intelligent control strategy". *Journal of Computing, 35*, 121–134, 2024.

[20] M. I. Solihin, L. F. Tack, & M. L. Kean. "Tuning of PID controller using particle swarm optimization (PSO)". *International Journal on Advanced Science, Engineering and Information Technology, 1*(4), 458–461, 2011.